NJC

Electrocatalytic hydrogen production with [FeFe]-hydrogenase mimics by tetracene derivatives

New Journal of Chemistry

Electrocatalytic hydrogen production with [FeFe]-hydrogenase mimics by tetracene derivatives

Motonori Watanabe,*[a] Kenta Goto,[b] Takaaki Miyazaki,[c] Masahiko Shibahara,[d] Yuan Jay Chang,[e] Tashin J. Chow,[e] and Tatsumi Ishihara[a,f]

The synthesis, structure, physical property, and electrocatalytic hydrogen production of tetrathia-tetracene ligand based [FeFe]-hydrogenase mimic molecules were investigated. By adjusting the amount of iron, mono- and bis-[FeFe] coordinated complexes **1** and **2** were synthesized. The structures of **1** and **2** were analysed by NMR, IR, absorption spectra, cyclic voltammogram, and DFT computation analyses. In DFT electron density maps, the HOMOs and LUMOs were located at tetrathia-tetracene units, indicated that these complexes remain mainly acene characteristics. When weak acid of Et_3NHBF_4 was added to the CH_2Cl_2 solutions of **1** or **2**, the reductive potential of iron complexes was shifted to more positive values proportional to the concentration of acid. As the acid concentration increased, the current of reductive wave also increased, indicating the occurrence of catalytic proton reduction reaction. The bulk electrolysis reaction showed 65.8 TON for **1**, and 52.8 TON for **2**.

Introduction

Hydrogen is the center of attraction as a next-generation energy carrier that will replace fossil fuels. Hydrogenases are among the most effective catalysts for the production of hydrogen, because they exhibit better hydrogen production activity than platinum [1,2]. The cost can also be reduced as compared to conventional catalysts such as platinum. The [FeFe]-hydrogenase has an Fe_2S_2 core that has been identified by X-ray diffraction analysis [3,4]. It is the activation center of hydrogen production, and its function has been studied by synthesizing molecules mimicking the Fe_2S_2 core [5,6]. Molecular structures containing dithiol group have been selected especially as the mimics [7]. Mimic molecules containing aromatic group with thiol group ligand have also been abundant, such as benzene derivatives [8-11], naphthalene derivatives [12],

naphthalene monoimide derivatives [13,14,22], pyridine derivatives [15], fluorene analogous [16,17], and phenanthrene derivatives [18]. These mimic molecules showed effective catalytic electro/photo chemical hydrogen productivities. Thus, investigations of [FeFe] hydrogenase mimetic molecules with new ligands play a key role in the research of molecular catalytic systems. Acenes are molecules that contain linearly condensed benzene rings, which exhibit unique charge redox behaviour. It is known that acenes can form dithiol structures by treatment with sulfur [19-21]. In this report, we use tetrathiatetracene (**3**) [22] with bis-dithiol substituents as a new type of ligand for mimicking the structure of [FeFe]hydrogenase. By reacting with iron carbonyls, new iron complexes possessing mono and bis Fe_2S_2 units are synthesized (Figure 1). These complexes were found to be stable in both solid and solution state. We investigated their physical properties and hydrogen production activity by electrocatalysis. This is the first report on the catalytic activity of hydrogenase mimic iron complex containing a tetracene moiety.

[a.] International Institute for Carbon-Energy Research (I2CNER), Kyushu University, 819-0385, Motooka 744, Nishi-ku, Fukuoka, Japan. mwata@i2cner.kyushu-u.ac.jp
[b.] Institute for Materials Chemistry and Engineering, Kyushu University, 744 Motooka, Nishi-ku, Fukuoka 819-0395, Japan
[c.] Department of Chemistry and Biochemistry, Graduate School of Engineering, 744 Motooka Nishi-ku, Fukuoka 819-0395, Japan
[d.] Division of Natural Sciences, Faculty of Science and Technology, Oita University, Dannoharu 700, Oita, Japan.
[e.] Department of Chemistry, Tunghai University, Taichung 40704, Taiwan
[f.] Department of Applied Chemistry, Faculty of Engineering, Kyushu University, Nishi-ku, Fukuoka 819-0395, Japan
Electronic Supplementary Information (ESI) available: Figure S1: IR spectra of complexes with 25 mM Et_3NHBF_4, Figure S2: Cyclic voltammetry of Et_3NHBF_4, Figure S3: Absorption spectra of complex solutions after bulk electrolysis, Table S1: X-ray crystallographic data]. See DOI: 10.1039/x0xx00000x.

Figure 1. Structure of **1** and **2** in this study

Results and discussion

Synthesis and characterization of iron complexes 1 and 2

[FeFe]-hydrogenase mimic molecules **1** and **2** were synthesized according to Scheme 1. The mono-[FeFe] coordinated complex **1** and bis-[FeFe] coordinated complex **2** can be obtained by adjusting the relative amounts of triirondodecacarbonyl and tetrathiotetracene **3**. The dark-green complex **1** was obtained by heating triirondodecacarbonyl (0.4 equiv.) with **3** in toluene solution (15% based from $Fe_3(CO)_{12}$). Complex **2** was obtained by the same synthesis method using 2 equiv. of triirondodecacarbonyl, and was isolated as a dark-blue powder (15% based from **3**).

Scheme 1. Synthesis of [FeFe]-hydrogenase mimic molecules **1** and **2**.
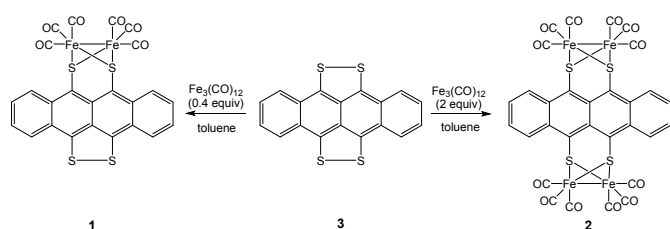
The structure of complexes **1** and **2** was confirmed by MS-spectra, ^{1}H and ^{13}CNMR, IR spectra, and X-ray crystallographic analyses. HRFAB-MS spectra of **1** showed m/z = 631.7950 (M+, calc. 631.7903) and **2** showed m/z = 911.6291 (M+, calc. 911.6296). Figure 2 showed the ^{1}HNMR spectra of **1-3**. The ^{1}H NMR spectra of parent structure **3** showed the aromatic proton peaks of at 7.43 and 7.30 ppm, respectively. The ^{1}H NMR spectra of complex **1** showed four independent aromatic peaks at 9.45, 7.90, 7.80, and 7.51 ppm, while those of complex **2** showed two independent peaks at 9.22 and 7.70 ppm, respectively.
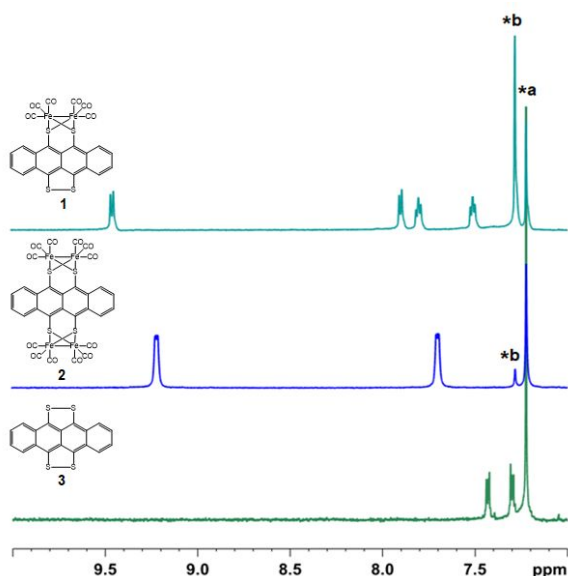
Figure 2. ^{1}HNMR spectra of **1-3** in $CDCl_3$:CS_2 = 2:3. Asterisks indicate solvent peaks (*a: $CHCl_3$, *b: benzene).

The infrared carbonyl stretching frequencies are affected by electronic interactions from ligand. [23] The $C \equiv O$ stretching modes in IR spectra of **1** in CH_2Cl_2 solution showed three peaks at 2068, 2033 and 1994 cm^{-1}, and those of **2** at 2070, 2045 and 2002 cm^{-1} (Figure 3). These values were similar with other reported PAH ligands [FeFe] complexes [24]. The $C \equiv O$ stretching frequency of **1** is lower than that of **2**, suggesting that the tetracene unit can donate more electron density to the mono Fe-S coordination. [24,25] The effect is consistent with the result of DFT computation at BP86/6-311G(d) level using CH_2Cl_2 solvated model. It showed that the averaged Mulliken charge (|e|) on the CO groups of **1** was more negative (-0.553 on C, -0.068 on O) than those of **2** (-0.544 on C, -0.049 on O).
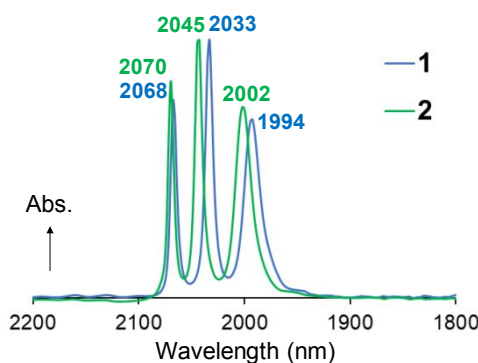
Figure 3. IR spectra of **1** and **2** in CH_2Cl_2 solution.

Crystallography
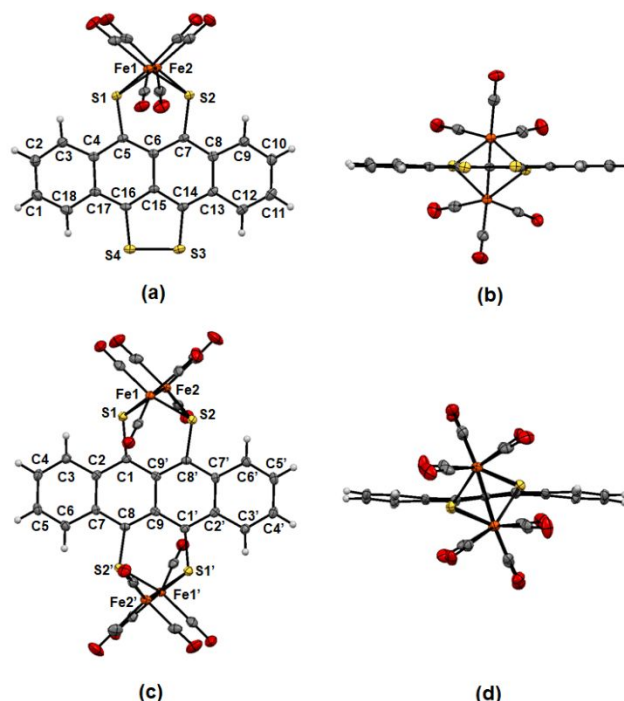
Figure 4. Crystal structures of **1** (a) top view and (b) side view, and **2** (c) top view and (d) side view. For structure 1, the incorporated solvent was omitted for clearly.

ARTICLE

Suitable single crystals of **1** and **2** suitable for X-ray crystallographic analyses were grown through slow evaporation of benzene solutions. Figure 4 showed the crystal structures of **1** and **2**. The structure of tetracene derivative **3** and its electronic properties have been reported [26-28]. In compound **3** the bond distance of S-S bond was found to be 2.100 Å [26]. In complex **1**, the distances of S3-S4 was estimated to be 2.068 Å, which indicated that the S3-S4 distance of **2** is also shorter than that of **3**. The distances of S1-S2 (S1'-S2') in **1** and **2** were found to be 2.997 and 2.967 Å, while those of Fe1-Fe2 (Fe1'-Fe2') were 2.512 and 2.518 Å, respectively. These distances were in good agreement with the S-S bond distances (2.94-3.02 Å) and the Fe-Fe bond distances (2.48-2.54 Å) in related diiron aryl-dithiolates [9,12,18]. The central two rings of the tetracene unit of **1** [containing atoms C4-C5-C6-C7-C8-C13-C14-C15-C16-C17] are coplanar. It forms slightly different dihedral angles with the two outside rings, i.e., 2.66° with the ring containing [C1-C2-C3-C4-C17-C18] and 0.66° with the one containing [C8-C9-C10-C11-C12-C13], and the dihedral angle of **2** between [C1-C2-C7-C8-C9-C9'-C8'-C7'-C2'-C1'] and [C2-C3-C4-C5-C6-C7] ([C2'-C3'-C4'-C5'-C6'-C7']) was 7.13°, respectively. The bending of tetracene moieties at **1** and **2** indicates that introducing the bulky groups of iron carbonyl twists the tetracene ligand skeleton. The average of C≡O distance is 1.388 Å for **1**, while 1.398 Å for **2**.

Absorption spectra
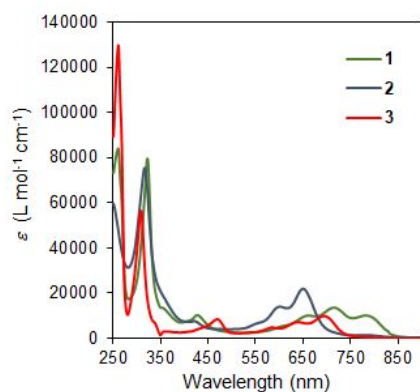
Figure 5. Absorption spectra of **1-3** (10^{-5} M) in CH_2Cl_2

The parent molecule of tetrathiatetracene **3** in CH_2Cl_2 solution absorbs at 697 (ε: 9900), 638 (ε: 7200), and 585 (ε: 4900) nm. After introducing of iron carbonyl groups into **3**, the absorption peaks shifted. The absorption of **1** in CH_2Cl_2 solution shows 789 (ε: 9600), 719 (ε: 13200), 660 (ε: 9800), and 601 (ε: 4900) nm, while **2** in CH_2Cl_2 solution shows 650 (ε: 21700), 598 (ε: 13700), and 559 nm (ε: 6700) nm, respectively (Figure 5). The DFT optimized structure at BP86/6-311G(d) level with CH_2Cl_2 solvated model showed the peaks of C≡O stretching modes at 2044, 2004 and 1964 cm^{-1} for **1**, and 2052, 2020 and 1972 cm^{-1} for **2**. The peak absorption frequency of **1** was lower than that of **2**. The trend of calculated IR values was consistent with the experimental values. Therefore, a theoretical analysis on the absorption spectrum can be performed based on optimized structures. The TDDFT computation at PBE0/6-311G(d)//BP86/6-311G(d) level using CH_2Cl_2 solvated model

showed that the 1st excited absorption wavelength of **1** was 644 nm (f = 0.1855, HOMO-LUMO), while the 1st excited absorption wavelength of **2** was 628 nm (f = 0.2539, HOMO-LUMO). The absorption peaks along with their oscillator strength were well agreed with experimental results. The visual molecular orbitals of **1** and **2** are shown in Figure 6. The HOMO and LUMO of **1** were delocalized at the tetracene and dithio group moieties not coordinated with iron-carbonyl. On the other hand, the HOMO and LUMO of **2** were delocalized mainly along the tetracene moiety, while the electron density was lower at the two dithio groups coordinated with iron carbonyl. For this reason, it can be predicted that the absorption band attributable to the π-π* transition of **2** appeared on the short wavelength side of **1**.

DFT computation
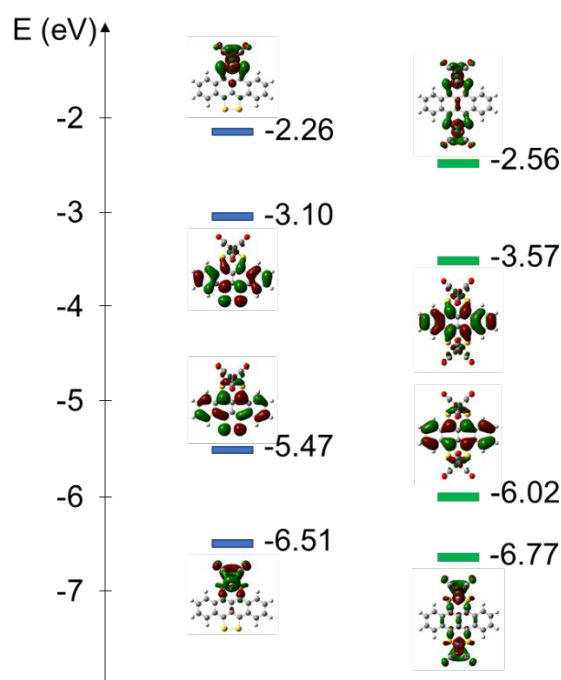
Figure 6. DFT computation results (BP86/6-311Gd level) of molecular diagram orbitals of **1** (left) and **2** (right).

Electrochemical properties

The electrochemical properties of **1** - **3** were performed. The carbon grassy was used as working electrode, platinum wire was used as counter electrode, and Ag/AgNo$_3$ was used as reference electrode. The potential was calibrated by ferrocene/ferrocenium potential in CH_2Cl_2 solution using nBu$_4$NPF$_6$ (0.1 M) as electrolyte. Due to low solubility, cyclic voltammogram of **3** was measured in a saturated CH_2Cl_2 solution containing nBu$_4$NPF$_6$ (0.1 M) as electrolyte at 313 K. Two irreversible reduction potentials were detected at -1.44 and -1.89 V, which were assigned to the reduction of S-S moiety (Figure 7a). The voltammogram features of **1** and **2** in CH_2Cl_2 solutions (1 mM at 298K) are shown in Figure 7b. One quasi-reversible reduction wave at -1.33 V and one irreversible reduction wave at -2.14 V were observed for **1**, while two quasi-reversible reduction waves at -1.05 and -1.39 V, and one irreversible reduction wave at -

2.21 V were observed for **2**. For metal-free ligand **3**, an irreversible reduction wave associated with the S-S bond was observed, whereas for complex **1**, the reduction wave corresponding to the ligand S-S moiety was observed to be quasi-reversible. This seems to indicate that the formation of iron complex stabilizes the S-S bond. In the X-ray-resolved crystal structure (Figure 4), the S-S bond distance of **1** was shorter (2.068 Å) than that of **3** (2.100 Å). It is suggested that the stability of the S-S bond of **1** is increased.

 The quasi-eversible waves of **1** and **2** were assigned to the reduction of tetrathiatetracene ligand. The irreversible waves were assigned to the reduction of $Fe^1Fe^1 \rightarrow Fe^1Fe^0$. The $Fe^1Fe^0 \rightarrow Fe^0Fe^0$ potential could not be determined due to outside solvent potential window. The reduction potentials of diiron moiety can be reduced by modifying the electronic structure of ligand, such as introducing electron withdrawing groups, [11,14,25] or changing the carbonyl moiety to a redox active phosphine moiety [29, 30]. The observed $Fe^1Fe^1 \rightarrow Fe^1Fe^0$ reduction potentials were higher than previously reported diiron dithiolates complexes (Table 1, -1.58 ~ -1.93 V vs Fc/Fc+)[12,14]. In the presence of acid Et_3NHBF_4 [29], the original peaks at -2.14 V for **1** and at -2.21 V for **2** were shifted to more positive. As acid concentration increased, the peak currents of **1** and **2** increased. These peak profiles on complex **1** and **2** show two processes: the first at −1.61 V for **1**, -1.34 V for **2**, and the second at -2.15 V for **1**, and -2.05 V for **2**, respectively (Figure. 8). IR spectra of **1** and **2 in** the presence of 25 mM Et_3NHBF_4 in CH_2Cl_2 showed no change on $C \equiv O$ stretching frequency, indicates that protonation did not occur at the ground state of **1** and **2** (Figure S1). In the absence of complexes **1** and **2**, the reduction of Et_3NHBF_4 did not occur in CH_2Cl_2 up to -2.5 V (Figure S2). It reveals that the increase of current upon the addition of Et_3NHBF_4 may be ascribed to the protonation of the reduced species of complexes **1** and **2**.
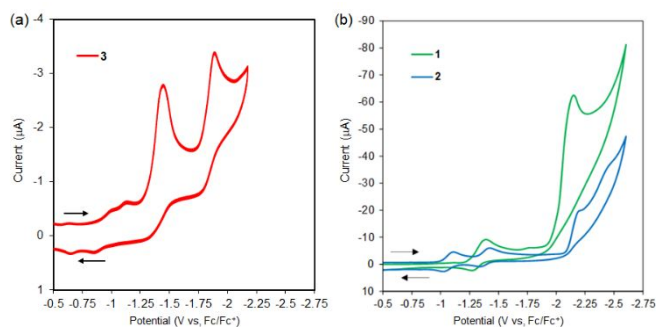
Figure 7. Cyclic voltammogram of (a) **3** (saturated at 313 K), **1** (1 mM at 298K) and **2** (1 mM at 298K) in CH_2Cl_2 with 0.1 M Bu_4NPF_6 as a supporting electrolyte at a scan rate of 100 mV/s.

The bulk electrolysis reaction of complexes **1** and **2** for catalytic hydrogen production was investigated. Based on the catalytic curve with acid (*p*-toluene sulfonic acid) in cyclic voltammetry, proton reduction rates of turn over frequency (TOF) were estimated by 4.5 ± 0.2 h^{-1} for the $[Fe_2(CO)_6(S_2C_6H_4)]$, and 3.1 ± 1.1 h^{-1} for the $[Fe_2(CO)_6(S_2C_{10}H_6)]$ [24].

Table 1. The reduction potentials of **1**-**3** and related complexes, estimated by cyclic voltammogram in CH_2Cl_2 with Bu_4NPF_6 (0.1 M) as the supporting electrolyte

Compounds	E_{pc} (V) ligand	E_{pc} (V) $Fe^1Fe^1 \rightarrow Fe^1Fe^0$	E_{pc} (V) $Fe^1Fe^0 \rightarrow Fe^0Fe^0$
$Fe_2(CO)_6(S_2C_3H_7)$ [12,14]		-1.93	
$Fe_2(CO)_6(S_2C_6H_4)$ [12]		-1.58 [$E_{1/2}$= -1.47]	
$Fe_2(CO)_6(S_2C_{10}H_6)$ [12]		-1.76 [$E_{1/2}$= -1.67]	**-2.00**
1	-1.38 [$E_{1/2}$= -1.33]	-2.14	
2	--1.10, -1.42 [$E_{1/2}$= -1.05, -1.39	-2.21	
3	-1.44, -1.89		

When bulk electrolysis reaction was performed in a CH_2Cl_2 solution containing only Et_3NHBF_4 (25 mM) and nBu_4NPF_6 (0.1 M), no hydrogen was detected. When the reaction was performed at -2.0 V vs Fc/Fc+ by 1.0 mM of **1** or **2** in CH_2Cl_2 solutions with Et_3NHBF_4 (25 mM) as the proton source and nBu_4NPF_6 (0.1 M) as the electrolyte, 32.9 mmol of H_2 was obtained after 24 h for **1** (based on TCD-GCMS), and 26.4 mmol of H_2 was detected after 24 h for **2** (based on thermal conductivity detector - gas chromatography mass spectrometry (TCD-GCMS)).
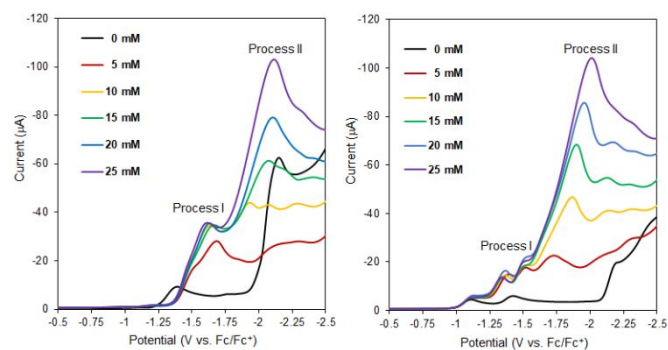
Figure 8. Cyclic voltammogram of **1** (1.0 mM at 298 K) and **2** (1.0 mM at 298 K) with different concentration of acid Et_3NHBF_4 in 0.1 M Bu_4NPF_6 as a supporting electrolyte at a scan rate of 100 mV/s.

After the reaction, both **1** and **2** showed a decrease of intensity in the absorption spectrum. The amount of decrease indicated that **2** was more stable under bulk electrolysis condition (Figure S3). This reveals that, the non-coordinated S-S bond of **1** is cleaved more easily. Based on the amount of hydrogen production, the turn over

ARTICLE

numbers (TONs) were estimated to 65.8 TON for **1** (TOF = 2.7 h^{-1}), and 52.8 TON for **2** (TOF = 2.2 h^{-1}). After the reaction, These TON values were comparable with previous reported [Fe$_2$(CO)$_6$(1,2-S$_2$C$_6$H$_4$)] and [Fe$_2$(CO)$_6$(S$_2$C$_{10}$H$_6$)] molecular catalysts.

General

The ^{1}H NMR spectra were recorded on a BrukerAV600 (600 MHz) spectrometer. The ^{1}H NMR chemical shifts were reported as δ values (ppm) relative to external Me$_4$Si. The coupling constants (*J*) were given in hertz. High resolution FAB mass spectra were recorded on a JMS-700 MStation spectrometer using 3-nitrobenzyl alcohol (NBA) as the matrix. Analytical thin layer chromatography (TLC) was performed on Silica gel 60 F254 Merck. Column chromatography was performed on KANTOSi60N (neutral). Absorption spectra were recorded on a SIMADZU UV-3600. For the measurements of absorption coefficient, a concentration of 1.0 × 10^{-5} M with an optical path length of 10 mm was used; and for the measurements before and after the bulk electrolysis, an optical path length of 1 mm was used. IR spectra were performed by SHIMADZU IRPrestige-21 spectrophotometer. All solvents and reagents were of reagent quality, purchased commercially, and used without further purification. CV measurements were performed using a cell equipped with glassy carbon as the working electrode, platinum wire as the counter electrode, and Ag/AgNO$_3$ as the reference electrode in CH$_2$Cl$_2$ solutions (1 × 10^{-3} M) containing 0.1 M tetra-n-butylammonium hexafluorophosphate (Bu$_4$NPF$_6$) as a supporting electrolyte at a scan rate of 100 mV/s. Bulk electrolysis (at -2.0 V vs Fc/Fc$^+$) was performed using a closed cell (VB1-4, cell volume: 37.4 mL, EC FRONTIER, Japan) equipped with glassy carbon (7.07 cm^2) as the working electrode, platinum wire as the counter electrode, and Ag/AgNO$_3$ as the reference electrode, in 10 mL CH$_2$Cl$_2$ solutions (1 × 10^{-3} M) containing 0.1 M Bu$_4$NPF$_6$ as a supporting electrolyte. The amount of H$_2$ gas was measured with a TCD gas chromatograph (GC-8A, Molecular Sieve 5A, Ar carrier, Shimadzu Corp., Japan), Dead volume was 27.4 mL. THF was distilled from sodium benzophenone ketyl. CH$_2$Cl$_2$ and toluene were distilled from CaH$_2$ under N$_2$ atmosphere. DFT computations were executed by Gaussian G09 Rev C. 01 software. Chemical structures were optimized by DFT at BP86/6-311G(d) level with CH$_2$Cl$_2$ solvated model, while no imaginary structure was found. while TDDFT computations were calculated at PBE0/6-311G(d)//BP86/6-311G(d) level.

Synthesis

Synthesis of mono-iron complex 1

A mixture of tetrathiotetracene **3** (705 mg, 2.00 mmol), triirondodecacarbonyl (402 mg, 0.80 mmol), anhydrous toluene (300 mL) was refluxed 1h under Ar atmosphere. After reaction, the reaction mixture was filtered, and the filtrate was evaporated to 100 mL, then filtered again to remove unreacted **3**. The green colour solution was evaporated to ca. 30 mL, and the precipitates were collected as a mixture of **1** and **3**. An amount of unreacted **3** was separated by dissolving in CH$_2$Cl$_2$, then the filtrate was recrystalized by benzene. Pure **1** was obtained as dark green solid (76.9 mg, 15%, based from triirondocecacarbonyl). Physical data of **1**: δH

(CDCl$_3$:CS$_2$ = 2:3, 600 MHz) 9.45 (m, 2H), 7.90 (m, 2H), 7.80 (m, 2H), and 7.51 (m, 2H); ν(KBr, CH$_2$Cl$_2$) 2068, 2033, 1994 (C ≡ O) cm^{-1}; HRMS (FAB) m/z [M]$^+$: calcd for C$_{24}$H$_8$Fe$_2$O$_6$S$_4$: 631.7903; found: 631.7950

Synthesis of bis−iron complex 2

A mixture of tetrathiotetracene **3** (1.16 g, 3.29 mmol), triirondodecacarbonyl (3.31 g, 6.58 mmol), anhydrous toluene (300 mL) was refluxed 1h under Ar atmosphere. After reaction, the reaction mixture was filtered, then the filtrated was concentrated to 30 mL. The precipitates were corrected, then recrystalized by benzene, to give pure **2** as dark blue solid (452 mg, 15%, based from **3**).

Physical data of **2**: δH (CDCl$_3$:CS$_2$ = 2:3, 600 MHz) 9.22 (dd, *J* = 6.7, 2.6 Hz, 4H) and 7.70 (dd, *J* = 6.9, 2.9 Hz, 4H); ν(KBr, CH$_2$Cl$_2$) 2070, 2045, 2002 (C ≡ O) cm^{-1}; HRMS (FAB) m/z [M]$^+$: calcd for C$_{30}$H$_8$Fe$_4$O$_{12}$S$_4$: 911.6296; found: 911.6291

Crystallography

Crystallographic data of the structures reported in this paper have been deposited with the Cambridge Crystallographic Data Centre as supplementary publication CCDC 1915438 (**1**) and CCDC 1915667 (**2**). Copies of the data can be obtained free of charge on application to CCDC, 12 Union Road, Cambridge CB2 1EZ, UK (Fax: + 44 1223 336 033; e-mail: deposit@ccdc.cam.ac.uk).

Summary

The [FeFe]-hydrogenase mimic molecules based on tetrathia-tetracene ligands were synthesized. By adjusting the relative amount of iron carbonyl, mono- and bis-[FeFe] coordinated complexes were obtained. The structures of **1** and **2** were analysed by NMR, IR, and absorption spectra, as well as cyclic voltammogram and DFT computational analyses. The HOMOs and LUMOs of **1** and **2** were found to locate mainly at the tetrathia-tetracene moiety. It suggested that these complexes maintain mostly the acene characteristics. When weak acid was added to the solutions of **1** or **2**, the original reductive waves of Fe^{1}Fe^1 -> Fe^{1}Fe^0 were shifted to more positive field. The catalytic proton reduction with **1** and **2** in the presence of acid were also investigated by using of cyclic voltammetry and bulk electrolysis. New peaks appeared in accord to the concentration of acid, probably derived from protonation of the reduced species of complexes **1** and **2**. As the acid concentration increased, the peak current of **1** and **2** became larger, indicated that catalytic proton reduction reaction occurred. The bulk electrolysis reaction showed 65.8 TON (TOF = 2.7 h^{-1}) for **1**, and 52.8 TON (TOF = 2.2 h^{-1}) for **2**. These TON values confirmed the occurrence of catalytic reaction. The bis-diiron complex **2** showed higher stability than **1** under bulk electrolysis, yet the catalytic hydrogen productivity was not enhanced. In this report we demonstrated for the first time that [FeFe]-hydrogenase mimic molecules with tetracene-based ligands are effective for the electrochemical catalytic hydrogen production.

Conflicts of interest

There are no conflicts to declare.

Acknowledgements

References

[1] M. Frey, *Chembiochem*, **2003**, *3*, 153-160.

[2] T. Matsumoto, S. Eguchi, H. Nakai, T. Hibino, K.-S. Yoon, S. Ogo, *Angew. Chem. Int. Ed*., **2014**, *53*, 8895-8898.

[3] J. W. Peters, W. N. Lanzilotta, B. J. Lemon, L. C. Seefeldt, *Science*, **1998**, *282*, 1853-1858.

[4] Y. Nicolet, C. Piras, P. Legrand, C. E. Hatchikianm, J. C. Fontecilla-Camps, *Structure,* **1999**, *7*, 13 -23.

[5] F. Gloaguen, J. D. Lawrence, T.B. Rauchfuss, *J. Am. Chem. Soc,.* **2001**, *123*, 9476-9477.

[6] L.C. Song, B. Gai, H.T. Wang, Q. M. Hu, *J. Inorg. Biochem,* **2009**, *103*, 805-812.

[7] M. Watanabe, Y. Honda, H. Hagiwara, T. Ishihara, *J. Photochem. Photobiol. C,* **2017**, *33*, 1-26.

[8] D. Chong, L. P. Georgakaki, R. Mejia-Rodriguez, J. Sanabaria-Chinchilla, M. P. Soriaga, M. Y. Daremsbourg, *Dalt. Trans.,* **2003**, 4158-4163.

[9] G. A. N. Felton, A. K. Vannucci, J. Chen, L. T. Lockett, N. Okumura, B. J. Petro, U. I. Zakai, D. H. Evans, R. S. Glass, D. L. Lichtenberger, *J. Am. Chem. Soc.,* **2007**, *129*, 12521-12530.

[10] J. F. Capon, F. Gloaguen, P. Schollhammer, J. Talarmin, *J. Electrochemical. Chem*., **2004**, *566*, 241-247.

[11] E. S. Donovan, J. J. McCormick, G. S. Nichol, G. A. N. Felton, *Organometallics*, **2012**, *31*, 8067-8070.

[12] R. J. Wright, C. Lim, T. D. Tilley, *Chem. Eur. J.* **2009**, *15*, 8518-8525.

[13] A. P. S. Samuel, D. T. Co, C. L. Stern, M. R. Wasielewski, *J. Am. Chem. Soc.,* **2010**, *132*, 8813-8815.

[14] H. Abul-Futouh, A. Skabeev, D. Botteri, Y. Zagranyarski, H. Görls, W. Weigand, K. Peneva, *Organometallics,* **2018**, *37*, 3278-3285.

[15] J. Chen, A. K. Vannucci, C. A. Mebi, N. Okumura, S. C. Borowski, M. Swenson, L. T. Lockett, D. H. Evans, R. S. Glass, D .L. Lichtenberger, *Organometallics*, **2010**, *29*, 5330-5340.

[16] R. Goy, L. Bertini, H. Görls, L. D. Gioia, J. Talarmin, G. Zampella, P. Schollhammer, W. Weigand, *Chem. Eur. J.* **2015**, *21*, 5061-5073.

[17] R. Goy, U. P. Apfel, C. Elleouet, D. Escudero, M. Elstner, H. Görls, J. Talarmin, P. Schollhammer, L. Gonzá lez, W. Weigand, *Eur. J. Inorg. Chem.* **2013**, 4466-4472.

[18] C. A. Mebi, B.C. Noll. R. Gao, D. Karr, *Z. Anorg, Allog. Chem.* **2010**, *636*, 2550-2554.

[19] S. Ohnish, T. Nogami, H. Mikawa, *Tetrahedron Lett.,* **1983**, *24*, 2401-2402.

[20] H. Endres, H. J. Keller, J. Queckboerner, J. Veigel, D. Schweitzer, *Mol. Cryst. Liq. Cryst.,* **1982**, *86*, 1851-1862.

[21] A. L. Briseno, Q. Miao, M.-M. Ling, C. Reese, H. Meng, Z. Bao, F. Wudl, *J. Am. Chem. Soc.,* **2006**, *128*, 15576-15577.

[22] M. R. Garrett, M. J. Durán-Peña, W. Lewis, K. Pudzs, J. Užulis, I. Mihailovs, B. Tyril, J. Shine, E. F. Smith, M. Rutkis, S. Woodward, *J. Mater. Chem. C*, **2018**, *6*, 3403-3409.

[23] L. Schwartz, P. S. Singh, L. Eriksson, R. Lomoth, S. Ott, *C. R. Chimie,* **2008**, *11*, 875-889.

[24] R. J. Wright, C. Lim, T. D. Tilley, *Chem. Eur. J*, **2009**, *15*, 8518-8525.

[25] H. Abul-Futouh, Y. Zagranyarski, C. Müller, M. Schulz, S. Kupfer, H. Görls, M. El-khateeb, S. Gräfe, B. Dietzek, K. Peneva, W. Weigand, *Dalton Trans.,* **2017**, *46*, 11180–11191.

[26] O. Dideberg, J. Toussaint, *Acta Cryst.,* **1974**, *B30*, 2481-2485.

[27] D. L. Smith, H. R. Luss, *Acta Cryst.*, **1977**, *B33*, 1744-1749.

[28] S. Sekizaki, C. Tada, H. Yamochi, G. Saito, *J. Mater. Chem.,* **2001**, *11*, 2293-2302.

[29] R. Becker, S. Amirjalayer, P. Li, S. Woutersen, J. N. H. Reek, *Sci. Adv.* **2016**, *2*, e1501014.

[30] T. B. Rauchfuss, *Acc. Chem. Res.* **2015**, *48*, 2107–2116.